Modulation of interface modes for resonance-induced enhancement of the interfacial thermal conductance in pillar-based Si/Ge nanowires

Yingzhou Liu,[*] Yinong Liu,[*] Jincheng Yue, Long Xiong,[†] Lei-Lei Nian,[‡] and Shiqian Hu[§]
School of Physics and Astronomy, Yunnan University, 650091 Kunming, People's Republic of China

(Received 6 July 2023; revised 7 November 2023; accepted 5 December 2023; published 19 December 2023)

The interfacial thermal conductance (ITC) plays a crucial role in nanoscale heat transfer, and its enhancement is of great interest for various applications. In this study, we explore the influence of resonance on the interfacial modes in pillar-based Si/Ge nanowires through nonequilibrium molecular dynamics simulations, employing both empirical and machine-learning potentials. Our results reveal a significant enhancement in the ITC by introducing pillars in the nanowire structure. The resonance-induced enhancement of the matching degree of the phonon density of states together with the calculation results of the phonon transmission coefficient indicate a significant improvement in both elastic and inelastic phonon transport at the interface. Moreover, we demonstrate the effective utilization of resonance to modulate the interfacial modes in pillar-based Si/Ge nanowires, resulting in improved phonon transport efficiency. This modulation is achieved by strategically repositioning the Si and Ge walls near the interface, leading to the development of the ATI-wall structure. Remarkably, the ATI-wall structure exhibits an unprecedented increase in the ITC compared to the original pillar-based design. To provide additional support for our conclusion, we conduct supplementary simulations using graphics processing unit molecular dynamics in conjunction with the neuroevolution potential to calculate the ITC. Our findings highlight the significance of interfacial mode modulation in enhancing the heat transfer in nanoscale systems and provide valuable insights for the design and optimization of thermal management devices and materials.

DOI: 10.1103/PhysRevB.108.235426

I. INTRODUCTION

The rapid growth of highly integrated nanoscale devices driven by high-end chips and electronic components has posed a significant thermal management challenge due to miniaturization, escalating power density, and substantial heat accumulation. Effective strategies have been developed to overcome this heat dissipation bottleneck, including the modulation of phonon transport within nanomaterials and at the interfaces of heterogeneous materials. Strategies for controlling phonon transport in nanomaterials have been extensively explored, involving modulation of both the wave [1–3] and particle [4–6] nature of phonons. Among these methods, the local phonon resonance mechanism has gained significant attention for modulating phonon transport in nanometamaterials [7–15]. This strategy offers the advantage of exploiting phonon wave characteristics while minimizing negative impacts on electron transport [16–18].

On the other hand, the modulation of the interfacial phonon transport has emerged as a crucial aspect of thermal management. To enhance the interfacial thermal conductance (ITC), various strategies have been proposed, including the use of interfacial nanostructures [19–23], the introduction of intermediate materials [24–27], and the application of external strain [28–30]. However, limitations exist within these strategies. For example, the use of intermediate materials, although effective in some cases, may exhibit limitations when exposed to high temperatures, compromising their stability and durability [31].

Furthermore, despite extensive research on the ITC, a notable gap still exists in understanding the relationship between modal changes in phonon transport states and the enhancement of interfacial phonon transport. Additionally, the investigations into the specific influence of the resonance structures on the ITC have received limited attention. Therefore, it is crucial to explore the role of the resonance structures in regulating the phonon transport state and their potential impact on the interfacial phonon transport, bridging this gap and develop more effective and reliable strategies for thermal management.

Moreover, numerous studies have shown that when heterogeneous materials are brought together at their interface, a disruption of the translational symmetry occurs, leading to the emergence of the localized interfacial modes [32–39]. For instance, in Si/Ge heterostructures, these interfacial modes are primarily attributed to the Si-Ge bonds formed at the interface [37]. Notably, although these interfacial modes constitute less than 5% of the total modes, they have been found to contribute significantly, accounting for more than 15% of the ITC [32–34]. Moreover, these modes exhibit strong coupling with nearly all other modes [32,33,38], enabling effective energy exchange between heterogeneous interfaces. Specifically, through the process of inelastic transport, phonons originating from bulk counterparts interact with localized

[*]These authors contributed equally to this work.
[†]Corresponding author: xiongl@ynu.edu.cn
[‡]Corresponding author: llnian@ynu.edu.cn
[§]Corresponding author: shiqian@ynu.edu.cn

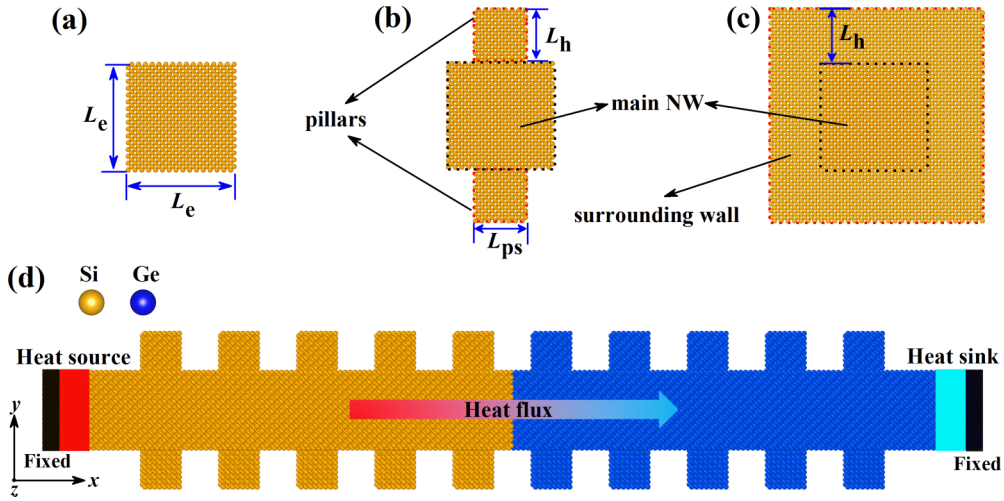

FIG. 1. Schematic of the pillar-based resonant structures and NEMD simulation model. The side views depict the periodic unit cell for (a) pristine Si/Ge NW, (b) two-side branched Si/Ge NW, (c) surrounding wall Si/Ge NW, and (d) the NEMD simulation model used for calculating the ITC.

phonons at the interface, thereby facilitating energy conversion [35,37,39]. As a result, the presence of these interfacial modes serves as a bridging mechanism that significantly enhances the ITC [35]. However, despite recognizing the crucial role of the interfacial modes in the interfacial phonon transport, there remains a limited emphasis on research aimed at effectively modulating these modes [40].

In this study, our objective is to comprehensively explore the role of the resonance in regulating the interfacial phonon transport in pillar-based Si/Ge nanowires, which are highly relevant to the field of thermal management in nanoscale devices. By employing the nonequilibrium molecular dynamics (NEMD) simulations, we analyze the effect of varying the number of pillars and the geometry of the structure on the ITC. Our simulations confirm the presence of resonance-induced phonon flat bands, which significantly promote the interfacial phonon transport through both elastic and inelastic mechanisms. This enhancement is further evidenced by the significant improvement in the matching degree of the phonon density of states (PDOS) and the phonon transmission coefficient. Additionally, we introduce an approach to further enhance the interfacial phonon transport by strategically moving the surrounding walls to the interface of the Si-Ge nanowires. This innovative method directly modulates the interfacial states, leading to a remarkable increase in the ITC. The enhanced phonon transport across the interface offers promising opportunities for improving thermal management and energy conversion in highly integrated nanoscale devices. Furthermore, we investigate the temperature dependence of the ITC and observe a significant increase in the slope, providing additional evidence of the resonance-induced enhancement of the inelastic phonon transport. These findings shed light on the modulation of the interfacial modes and their contribution to the ITC in pillar-based Si/Ge nanowires. By gaining valuable insights into these mechanisms, our research contributes to the development of more effective and reliable strategies for addressing the challenges associated with heat dissipation and energy conversion in nanoscale devices.

II. METHODS

A. Molecular dynamics simulations

The main Si/Ge nanowire (NW) employed in this study has a square cross section with an edge length L_e of 4.34 nm, as illustrated in Fig. 1(a). The side views of the periodic unit used to create the partial pillar-based resonant structures are shown in Figs. 1(b) and 1(c). Each side branch of the Si/Ge NWs consists of ten pillars, which have a square cross section with a pillar length L_{ps} of 2.17 nm and a fixed pillar height L_h of 2.17 nm. To investigate the influence of the number of pillars on the interfacial phonon transport, we construct Si/Ge NWs with varying numbers of branches, ranging from pristine (no branches) to four-side branched NWs. Additionally, a structure surrounded by walls is also included in the analysis.

The NEMD calculations in this study are implemented using the LAMMPS packages [41] for the empirical potential, while the machine-learning potential is executed with the graphics processing unit molecular dynamics (GPUMD) [42,43]. The interatomic interactions described in the LAMMPS between Si-Si, Ge-Ge, and Si-Ge are modeled using the Stillinger-Weber (SW) potential with Si parametrizations [44]. To simplify the simulation, Ge atoms were treated as "heavy Si" with a mass ratio of 2.59, considering the transferability of interatomic force constants between Si and Ge [37,45–48]. The boundary conditions in our simulations are as follows: free boundary conditions are applied in the y and z directions by adding a 100 Å vacuum layer in both directions. In contrast, a fixed boundary condition is employed in the x direction, where the positions of six Å Si or Ge atoms at two ends of the system are held fixed [indicated by the black region in Fig. 1(d)]. Two Langevin thermostats with different temperatures (T_H and T_L) are connected to the two ends of the simulation system to create a steady temperature distribution. In our simulations, we set $T_H = 320$ K and $T_L = 280$ K to calculate the ITC at 300 K. After the system reaches the steady state, the cumulative energy ΔE added/subtracted to the heat source/sink region is recorded for 5 ns. The time step is set as 0.5 fs. The energy change per unit time was obtained by

linearly fitting to the raw data of accumulated energy ΔE, which is used to calculate the heat flux $J = \Delta E/\Delta t$. The ITC G is calculated by $G = J/(S\Delta T)$, where S is the cross-sectional area and ΔT is the temperature difference. A typical heat flux calculation and temperature profiles are presented in Supplemental Material Fig. S1 [49]. These results are averaged over three independent simulations with different initial conditions. The error bars displayed on the graphs represent the standard deviations resulting from these three independent simulations.

B. Phonon properties calculations

The phonon transmission, denoted as $\Gamma(\omega)$, can be calculated using molecular dynamics calculation which accounts for all orders of the anharmonic interactions [50,51]. It is linked to the interfacial thermal conductance using the Landauer expression: $G(\omega) = \frac{k_B}{S}\Gamma(\omega)$ [52–54]. The expression for the phonon transmission is as follows:

$$\Gamma(\omega) = \frac{q(\omega)}{k_B \Delta T}, \tag{1}$$

where k_B is the Boltzmann constant, and ΔT represents the temperature difference between two Langevin thermostats. The $q(\omega)$ in the equation represents the heat flow across the cross section S, and it is calculated as follows [50,51]:

$$q(\omega) = \frac{2}{M\Delta t}\mathrm{Re}\sum_{i\in L}\sum_{j\in R}\langle \hat{\boldsymbol{F}}_{ij}(\omega)\hat{\boldsymbol{v}}_i(\omega)^*\rangle, \tag{2}$$

where Δt is the time interval between samples taken in the simulation, and M is the number of samples. The summation is carried out over atoms within a limited region of 1 nm from the interface on the left (L) and atoms on the right (R). This spatial constraint ensures that only atoms within this range are considered, as atoms beyond it do not interact with those on the opposite side of the interface. The quantities $\hat{\boldsymbol{F}}_{ij}(\omega)$ and $\hat{\boldsymbol{v}}_i(\omega)^*$ represent the Fourier transformation of the force and the velocity of the atom, respectively. The force $\boldsymbol{F}_{ij}$ is the total force exerted by the right atoms on the left atoms i at the interface and the Fourier transforms are defined for, e.g., the velocities as [50,51]

$$\hat{\boldsymbol{v}}_i(\omega_l) = \Delta t\sum_{k=1}^{M} e^{i\omega_l k\Delta t}\boldsymbol{v}_i(k\Delta t). \tag{3}$$

Note that the forces $\boldsymbol{F}_{ij}$ and velocities $\boldsymbol{v}_i$ are directly obtained during the execution of the molecular dynamics (MD) simulations. Consequently, in our simulations, the calculation of phonon transmission considers the anharmonic effect. This consideration allows us to capture the complex interactions and behavior of phonons, including their scattering and transmission properties, providing a more comprehensive understanding of the interfacial phonon transport in the studied system.

Furthermore, we calculate the PDOS to investigate the overlap factor between the two materials at the interface and determine the presence of interfacial modes [55–57]. The PDOS, denoted as $D(\omega)$, is determined using the following expression:

$$D(\omega) = \lim_{\tau\to\infty}\int_{-\tau}^{\tau}\frac{\left\langle\sum_{i=1}^{n} v_i(t)v_i(0)\right\rangle}{\left\langle\sum_{i=1}^{n} v_i(0)v_i(0)\right\rangle}e^{-i2\pi ft}dt, \tag{4}$$

where v_i represents the velocity of the ith atom, f is the frequency, n is the total number of atoms, t is the correlation time, and $\langle\cdots\rangle$ denotes an ensemble average. The crucial factor that governs phonon transport at heterogeneous interfaces is the matching degree of the PDOS [58–61]. This matching degree is quantified by the overlap factor S, which measures the similarity between the PDOS of the connecting materials using a cosine similarity measure [60],

$$S = \frac{\int D_1(\omega)D_2(\omega)d\omega}{\left[\int D_1(\omega)^2 d\omega\right]^{1/2}\left[\int D_2(\omega)^2 d\omega\right]^{1/2}}, \tag{5}$$

where $D_1(\omega)$ and $D_2(\omega)$ represent the PDOS of Si and Ge, respectively.

III. RESULTS AND DISSCUSSION

First, it is important to note that the system's size can significantly impact the specific value of the ITC. This phenomenon arises from the fact that shorter simulation domains may be influenced by thermal reservoirs, which can reflect transmitted phonons back to the interface, thereby affecting the ITC [62]. Therefore, we conduct calculations to explore the relationship between the ITC of pristine Si/Ge NW structures, in relation to the system's size. As depicted in Fig. S2, we observe a gradual increase in the ITC with an increase in the system size, which tends to converge when the system size exceeds 50 nm. This discovery aligns with prior findings [35]. Consequently, considering computational cost constraints, we adapt a system size of 50 nm for a significant portion of our subsequent calculations. As depicted in Fig. 2(a), the introduction of the pillars in the Si/Ge NWs results in a notable enhancement in the ITC. Moreover, the ITC exhibits a monotonically increasing trend with the number of the resonant branches, progressing from pristine to four-side branched and further to the surrounding wall NWs. This enhanced interfacial phonon transport behavior is distinctly different from previous studies where phonon resonance was utilized to induce a reduction in the thermal conductivity [10,12,13]. Notably, the resonance effect affects the phonon transport by flattening the phonon dispersion relationship, leading to the changes in the PDOS. While the flat bands have traditionally been considered detrimental to the phonon transport, as they have near-zero group velocities and limited energy transmission capabilities. However, in the context of interfacial phonon transport, these dispersionless phonon modes can play a significant role. Firstly, the resonance effects induce a notable downward shift of the phonon bands in both materials towards lower frequencies at the interface. This shift has the potential to affect the matching degree of the PDOS at the interface, thereby influencing the efficiency of the phonon transmission [58–61,63]. Secondly, although these flat band phonons themselves cannot contribute to the heat transfer directly, they can serve as carriers for phonon scattering events involving other phonons [35,37,39,40]. This mechanism promotes the inelastic scattering through multi-

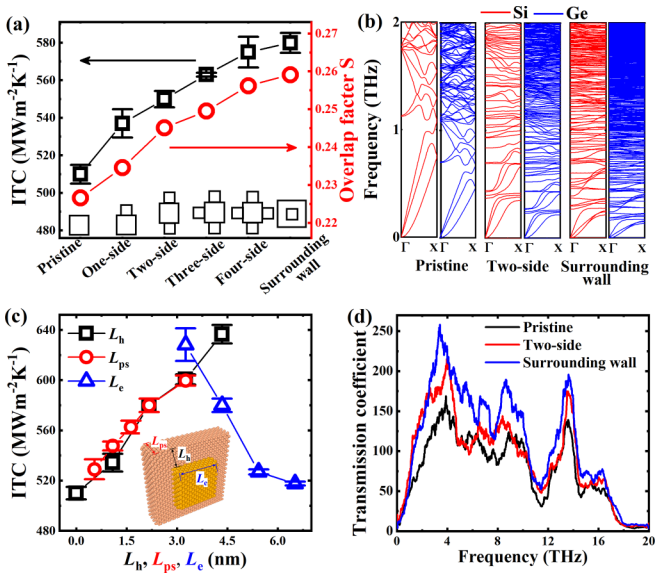

FIG. 2. Effect of the number and height of pillars on the interfacial phonon transport and related phonon characterization. (a) Impact of the number of pillars, ranging from pristine to four-side branched and further to surrounding wall NWs, on the ITC, with the $L_h = 2.17$ nm. The right y axis represents the corresponding overlap factor. (b) The dispersion relations for the pristine, two-side and surrounding wall NWs corresponding to the configurations in panel (a). (c) The effect of the geometry, such as pillar height L_h, pillar length L_{ps}, and edge length L_e for surrounding wall NWs on the ITC. (d) The transmission coefficients of the partial structures corresponding to the pillar configurations shown in panel (a).

phonon interactions, such as three-phonon and higher-order processes, facilitating the thermal transport across the interface.

Therefore, to further validate our inference regarding the impact of the flat bands on the interfacial phonon transport, and to explore the underlying physical mechanism behind the observed increase in the ITC, we conduct additional calculations to analyze the phonon dispersion relations of three representative Si and Ge structures. All the phonon dispersions are calculated using lattice dynamics implemented in the General Utility Lattice Program (GULP) [64]. Furthermore, the phonon dispersions are obtained using the periodic unit cells, as depicted in Figs. 1(a)–1(c). Notably, in the direction where the pillars are introduced, a 100-Å vacuum layer is included to preserve the resonance effect induced by the pillars for the two-side branched and surrounding wall nanowires. As depicted in Fig. 2(b), the introduction of the pillars in the system results in a notable flattening of the phonon dispersion curve. This flattening originates from the hybridization between the wave-number-independent vibration modes in pillars (local resonance) and the wave-number-dependent phonon modes in the main nanowire (see details in Fig. S3 in the Supplemental Material [49]) [7–10]. Additionally, the presence of more branched pillars causes a shift of the flat band towards lower frequencies, indicating the presence of stronger phonon resonances [10]. Moreover, our analysis of the overlap factor of the PDOS, as shown in Fig. 2(a) (right y axis), demonstrates that the downward shift of the flat bands significantly enhances the matching degree of the PDOS at the interface, thereby promoting efficient interfacial phonon transport.

Moreover, in prior studies exploring the modulation of the phonon transport through resonance, the geometry of the structure, including parameters such as pillar height L_h, pillar length L_{ps}, and edge length L_e, has been identified as a crucial factor in determining the position of the flat bands [8–10]. In addition to the number of pillars, these geometric parameters play a significant role. As a result, in our forthcoming research, we conduct further investigations to explore the influence of specific geometric parameters on the ITC. It is worth noting that in these calculations, we keep two of these parameters constant while varying the third to assess its impact on the overall ITC. As expected, we observe that surrounding wall nanowires with increased pillar heights exhibit a noticeable increase in the ITC [Fig. 2(c)]. This increase can be attributed to the corresponding increase in the volume ratio between the pillars and the main nanowires as L_h increases. This heightened volume ratio enhances the resonance effect, resulting in an increase in the ITC. These findings, in conjunction with the improved overlap factors of the PDOS, indicative of the elastic contribution, and the phonon transmission calculation, which partially reflects the inelastic contribution (as shown in Supplemental Material Fig. S4 [49]), offer further evidence that greater pillar heights enhance the phonon transmission efficiency. Consequently, this enhanced phonon transmission contributes to the observed increase in the ITC. Similarly, when the L_{ps} increases, the volume ratio between the pillars and the main nanowires increases, resulting in an increase in the ITC [Fig. 2(c)]. Conversely, altering the L_e leads to a decrease in the volume ratio, subsequently resulting in a decrease in the ITC [Fig. 2(c)].

Up to now, we have successfully modulated the interfacial phonon transport by manipulating the number of the pillars and the geometry of the structure. Additionally, we have provided a reasonable explanation by evaluating the overlap factor of the PDOS. However, it is crucial to acknowledge that the calculation of the overlap factor primarily focuses on the elastic scattering and provides limited insight into the inelastic scattering. In order to gain a comprehensive understanding of the contribution of the inelastic scattering mechanism in the resonant Si-Ge interfacial phonon transport, we will proceed with further calculations of the phonon transmission coefficient.

As depicted in Fig. 2(d), the phonon transmission coefficient exhibits a clear increase with an increasing number of the pillars, which aligns with the observed increase in the ITC. Specifically, within the cut-off frequency range (<11 THz) for the crystalline material Ge, the upward trend in the transmission coefficient is predominantly attributed to the enhanced overlap of the PDOS, indicative of the improved elastic phonon transport. Conversely, in the high-frequency range (>11 THz) where the inelastic phonon transport dominates, the phonon transmission shows a peak, and a significant increase is also observed across different numbers of pillars. In the pristine case, the peak is a result of the presence of the interfacial modes (refer to the interfacial modes in Supplemental Material Fig. S5 [49]), which have been recognized in previous studies for their substantial impact on the interfacial phonon transport, primarily through the inelastic scattering

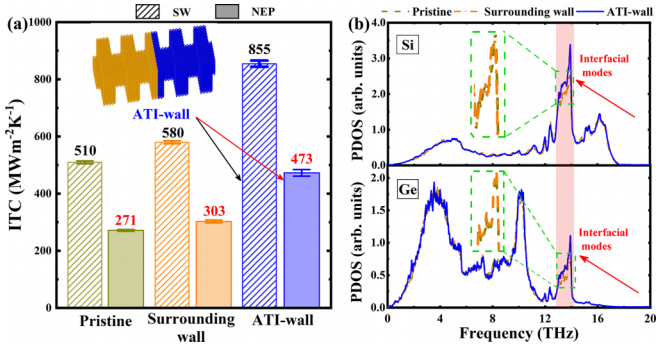

FIG. 3. The comparison of the ITC and corresponding PDOS for three representative structures. (a) The comparison of the ITC (calculated by the empirical SW potential and NEP machine-learning potential) among three structures: pristine, surrounding wall, and ATI-wall Si/Ge NWs. The inset shows the schematic of ATI-wall. (b) The difference in interfacial modes for the three structures depicted in panel (a), where the PDOS is calculated from the velocity of one layer of atoms at the interface.

mechanisms [32,33,35,37,38]. Upon introducing the pillars, the phonon dispersion curves undergo a downward flattening, resulting in an increased number of low-frequency phonons. These localized phonons play a similar role to the interfacial states by promoting the inelastic scattering, accounting for the higher and wider peaks observed at the high frequencies [37,39]. Moreover, we also employ an alternative method based on second-order force constants to calculate the phonon transmission coefficient (details provided in Supplemental Material Part I [49]). Interestingly, our calculations revealed no significant peaks in the high-frequency region beyond 11 THz (as illustrated in Supplemental Material Fig. S6 [49]). This finding can be attributed to the intrinsic limitations of the second-order force constant-based method, which does not consider anharmonic interactions and, as a result, lacks the capability to account for channels associated with inelastic scattering. Consequently, this result provides additional confirmation that the observed high-frequency peaks are indeed a result of inelastic scattering [65].

Through our research, we have discovered that both the resonance-induced flat bands and the unique interfacial states at the interface play a crucial role in facilitating the phonon transport through inelastic scattering mechanisms. These local states provide an additional pathway for the phonon transport across the interface, enhancing the ITC. However, previous studies have consistently demonstrated that the interfacial state is predominantly confined within one or two atomic layers at the interface of two materials [33,35,37]. In our above-mentioned structure, the closest pillars to the interface are located at a distance of 1 nm, which is not expected to directly influence the interfacial states. To investigate the influence of the resonance on the interfacial states, we make an additional modification to our structure. As depicted in the inset of Fig. 3(a), we reposition the Si and Ge walls adjacent to the interface, creating a novel structure known as the ATI-wall. The purpose of this modification is to explore the potential role of these walls in regulating the resonance of the interfacial states and examining its subsequent impact on the ITC.

The ITC of the ATI-wall structure, as shown in Fig. 3(a), demonstrates a remarkable increase compared to that of the previous surrounding wall structure. This substantial improvement implies the significant influence of resonance on the interfacial state and its impact on the interfacial phonon transport. To gain further insights into the underlying mechanism, we analyze the PDOS of one atomic layer at the interface for three structures: pristine, wall-surrounded NWs, and ATI-wall, as depicted in Fig. 3(b). Within the frequency range associated with the interfacial modes (pink shaded area), it is notable that the peaks of the PDOS for the pristine and surrounding wall NWs remain unchanged, while the ATI-wall exhibits a significant enhancement in the peaks of interfacial modes. This enhancement can be explained as follows: as mentioned earlier, the phonon resonance plays a crucial role in generating flat bands within the pillar-based structure. These flat bands exhibit significant similarities to the interfacial phonon modes in that they are localized states incapable of effectively propagating energy. However, it is crucial to note that these flat bands are not situated at the interface and, therefore, are not referred to as the interfacial phonon modes. In our ATI-wall structure, when the pillar is located at the interface, it essentially induces these localized states at the interface, thereby increasing the number of interfacial phonon modes. This observation suggests that placing the wall in close proximity to the interface allows for a pronounced influence of the phonon resonance on the number of interfacial modes present. This understanding underscores the importance of leveraging resonance to optimize the ITC and opens an avenue for the design and engineering of advanced thermal management materials and devices.

It is important to note that all the above results are based on the empirical SW potential, which is known to pose challenges in quantitatively describing the ITC. To ensure the reliability of our conclusion regarding the beneficial impact of introducing pillars on the ITC, we conduct additional simulations using GPUMD in combination with the neuroevolution potential (NEP) to calculate the ITC of the three representative structures. The NEP machine-learning potential field has previously demonstrated a level of accuracy comparable to that of density functional theory [66] (for details on the training of the NEP potential, please refer to Supplemental Material Part II [49]). As depicted in Fig. 3(a), the results of the ITC based on the NEP exhibit the same increasing trend as the simulations employing the SW potential field. It is noteworthy that the ITC values obtained using the NEP potential are lower than those from simulations employing the empirical SW potential. This difference is attributed to the SW potential's limited ability to describe phonon anharmonicity, suggesting the presence of phonon modes with extended relaxation times and leading to an overestimation of the numerical results [67]. However, these findings further emphasize the effectiveness of classical MD in qualitatively predicting relative trends and lend support to our conclusion.

On the other hand, in the context of the interfacial phonon transport, the interfacial modes and their associated inelastic scattering processes play a crucial role by significantly contributing to the overall ITC [37,39]. These modes, charac-

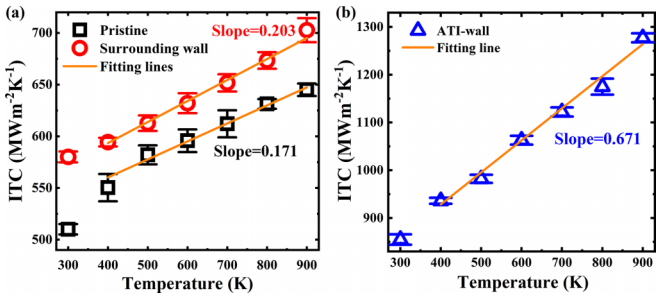

FIG. 4. The variation of the ITC with increasing temperatures in different structures, including (a) pristine and surrounding wall Si/Ge NWs and (b) ATI-wall Si/Ge NWs.

terized by localized vibrational states at the interface, become increasingly influential at higher temperatures. Notably, the behavior of the ITC at high temperatures provides valuable insights into the dominant scattering mechanism [37,39]. The convergence of the ITC suggests that elastic scattering predominantly governs the thermal transfer process, whereas a nonconverging ITC indicates the prevalence of the inelastic scattering [68–70].

To further investigate the impact of the interfacial modes on the inelastic transport, we conduct a detailed analysis of the temperature dependence of the ITC, as depicted in Fig. 4. Notably, the slope of the temperature-dependent ITC exhibits a greater value for the surrounding wall NWs (slope = 0.203) compared to the pristine structure (slope = 0.171) beyond the Debye temperature threshold of Ge (approximately 370 K) [71]. This observation strongly suggests a stronger inelastic transport in the surrounding wall structure, further confirming the existence and distinction of the high-frequency peak of the phonon transmission shown in Fig. 2(d). Furthermore, it is worth highlighting that the ITC of the ATI-wall structure displays an even steeper slope [slope = 0.671; Fig. 4(b)]. These results offer additional insights into the capacity of the resonance to modulate the interfacial modes and effectively enhance phonon interfacial phonon transport via inelastic scattering.

Furthermore, in addition to the interfacial thermal resistance (which is reciprocal of the interfacial thermal conductance) resulting from phonon-interface scattering, the role of thermal resistance between nonequilibrium phonons has garnered increasing attention [35,72–75]. This resistance is deeply influenced by phonon-phonon scattering [76]. Within our current structural configuration, the introduction of pillars in the main nanowire leads to the flattening of the bands and an increase in the number of interfacial phonon modes. These changes collectively exert a substantial impact on phonon-phonon scattering, particularly inelastic scattering [35,73,74]. Therefore, delving further into the implications of nonequilibrium phonons on the interfacial phonon transport within our current framework holds substantial value. This avenue of research warrants future exploration because it is an area still in its nascent stages, with no prior work attempting to modulate it. These investigations are essential for expanding and clarifying our comprehension of how to manipulate and control phonon nonequilibrium at the interface. Moreover, it is important to clarify that our primary focus in the current study is on interfacial thermal resistance induced by phonon-interface scattering. This thermal resistance is determined solely by the heat flux and the temperature jump across the interface. Consequently, the core conclusion of our study, which suggests that introducing pillars can effectively modulate both phonon elastic and inelastic scattering to enhance interfacial heat transport, remains valid.

Finally, the current study primarily investigates the impact of the resonance on the interfacial phonon transport, revealing stark differences compared to its effect on the thermal conductivity. Therefore, it is crucial to provide a brief exploration of the distinction between the thermal conductivity and the interfacial phonon transport, particularly within the framework of phonon resonance and further to the various phonon transport states. The thermal conductivity, as a concept, is more straightforward and aligned with the natural science, where the distinctions between various transport states are clear. In general, the ballistic transport surpasses the diffusive transport, which in turn exceeds the localization (may be induced by the resonance) in terms of the thermal conductivity. This intuitive relationship between the thermal conductivity and the phonon transport state can be established within the same material or structure.

However, the interfacial phonon transport presents a more philosophical challenge, as it necessitates the careful consideration of various factors, including the delicate balance of the PDOS, strength of interaction forces, interface roughness, interfacial bonding, interfacial chemistry, interface geometry, interfacial strain, and mass mismatch [19,20,23,31,63,65,77–83]. For instance, our previous work has revealed that interfaces with weak van der Waals forces can exhibit significantly higher thermal boundary conductance compared to those with strong covalent bonds in systems with a significant PDOS mismatch [77].

Therefore, the exploration of the interfacial phonon transport presents a profound challenge that necessitates a comprehensive understanding of various factors. In a remarkable breakthrough, our current research findings reveal the previously unrecognized positive influence of the resonance on the interfacial phonon transport. Through systematically studying the impact of the resonance on the interfacial states, we have gained valuable insights into the mechanisms through which these states affect the phonon transport at the interface. This groundbreaking discovery opens avenues for manipulating and controlling the interfacial phonon transport by harnessing the power of resonance. By comprehending the intricate nature of interfacial phonon transport, particularly the beneficial impact of the resonance, we not only advance our knowledge in the field but also unlock significant implications for the design and optimization of the thermal management materials and devices.

IV. CONCLUSIONS

In summary, our current work investigates the role of resonance in regulating the interfacial phonon transport in pillar-based Si/Ge nanowires for improved thermal management. Through the nonequilibrium molecular dynamics simulations, we analyze the effects of varying the number of pillars and the geometry of the structure on the ITC. The

results demonstrate a notable enhancement in the ITC by introducing pillars, attributed to the resonance-induced enhancement of the matching degree of the phonon density of states and the phonon transmission coefficient. Additionally, a novel structure called ATI-wall, achieved by strategically repositioning the Si and Ge walls near the interface, further enhances the ITC by directly modulating the interfacial states. The study provides valuable insights into the modulation of the interfacial phonon transport and its contribution to thermal management in nanoscale devices. These findings have significant implications for the design of advanced thermal management materials and devices, offering strategies to address the challenges associated with heat dissipation and energy conversion in highly integrated systems.

ACKNOWLEDGMENTS

This research was funded in part by the National Natural Science Foundation of China (Grants No. 12105242 and No. 12204405) and by Yunnan Fundamental Research Project (Grants No. 202201AT070161, No. 202301AW070006, and No. 202301AT070108). Y.L. and S.H. acknowledge support from the Graduate Scientific Research and Innovation Fund of Yunnan University (KC-22222049).

[1] M. N. Luckyanova, J. Garg, K. Esfarjani, A. Jandl, M. T. Bulsara, A. J. Schmidt, A. J. Minnich, S. Chen, M. S. Dresselhaus, Z. Ren, E. A. Fitzgerald, and G. Chen, Coherent phonon heat conduction in superlattices, Science **338**, 936 (2012).

[2] J. Ravichandran, A. K. Yadav, R. Cheaito, P. B. Rossen, A. Soukiassian, S. J. Suresha, J. C. Duda, B. M. Foley, C. H. Lee, Y. Zhu, A. W. Lichtenberger, J. E. Moore, D. A. Muller, D. G. Schlom, P. E. Hopkins, A. Majumdar, R. Ramesh, and M. A. Zurbuchen, Crossover from incoherent to coherent phonon scattering in epitaxial oxide superlattices, Nat. Mater. **13**, 168 (2014).

[3] S. Xie, L. Tu, Y. Han, L. Huang, K. Kang, K. U. Lao, P. Poddar, C. Park, D. A. Muller, R. A. DiStasio, Jr., and J. Park, Coherent, atomically thin transition-metal dichalcogenide superlattices with engineered strain, Science **359**, 1131 (2018).

[4] S. Chen, Q. Wu, C. Mishra, J. Kang, H. Zhang, K. Cho, W. Cai, A. A. Balandin, and R. S. Ruoff, Thermal conductivity of isotopically modified graphene, Nat. Mater. **11**, 203 (2012).

[5] Z. Tong, A. Pecchia, C. Yam, T. Dumitrica, and T. Frauenheim, Phononic thermal transport along graphene grain boundaries: A hidden vulnerability, Adv. Sci. **8**, e2101624 (2021).

[6] X. Chen, C. Li, Y. Xu, A. Dolocan, G. Seward, A. Van Roekeghem, F. Tian, J. Xing, S. Guo, N. Ni, Z. Ren, J. Zhou, N. Mingo, D. Broido, and L. Shi, Effects of impurities on the thermal and electrical transport properties of cubic boron arsenide, Chem. Mater. **33**, 6974 (2021).

[7] B. L. Davis and M. I. Hussein, Nanophononic metamaterial: Thermal conductivity reduction by local resonance, Phys. Rev. Lett. **112**, 055505 (2014).

[8] H. Honarvar and M. I. Hussein, Spectral energy analysis of locally resonant nanophononic metamaterials by molecular simulations, Phys. Rev. B **93**, 081412 (2016).

[9] H. Honarvar and M. I. Hussein, Two orders of magnitude reduction in silicon membrane thermal conductivity by resonance hybridizations, Phys. Rev. B **97**, 195413 (2018).

[10] S. Xiong, K. Saaskilahti, Y. A. Kosevich, H. Han, D. Donadio, and S. Volz, Blocking phonon transport by structural resonances in alloy-based nanophononic metamaterials leads to ultralow thermal conductivity, Phys. Rev. Lett. **117**, 025503 (2016).

[11] X.-K. Chen, J. Liu, Z.-X. Xie, Y. Zhang, Y.-X. Deng, and K.-Q. Chen, A local resonance mechanism for thermal rectification in pristine/branched graphene nanoribbon junctions, Appl. Phys. Lett. **113**, 121906 (2018).

[12] H. Zhang, B. Sun, S. Hu, H. Wang, Y. Cheng, S. Xiong, S. Volz, and Y. Ni, Novel phonon resonator based on surface screw thread for suppressing thermal transport of Si nanowires, Phys. Rev. B **101**, 205418 (2020).

[13] X. Wan, D. Ma, D. Pan, L. Yang, and N. Yang, Optimizing thermal transport in graphene nanoribbon based on phonon resonance hybridization, Mater. Today Phys. **20**, 100445 (2021).

[14] H. Wang, Y. Cheng, Z. Fan, Y. Guo, Z. Zhang, M. Bescond, M. Nomura, T. Ala-Nissila, S. Volz, and S. Xiong, Anomalous thermal conductivity enhancement in low dimensional resonant nanostructures due to imperfections, Nanoscale **13**, 10010 (2021).

[15] H. Liu, W. Li, Z. Cao, X. Huang, and Y. Ni, Enhanced phonon resonance by non-uniform surface nanopillars in Si nanowires, Int. J. Heat Mass Transfer **205**, 123903 (2023).

[16] M. I. Hussein, C. N. Tsai, and H. Honarvar, Thermal conductivity reduction in a nanophononic metamaterial versus a nanophononic crystal: A review and comparative analysis, Adv. Funct. Mater. **30**, 1906718 (2019).

[17] X. L. Shi, J. Zou, and Z. G. Chen, Advanced thermoelectric design: From materials and structures to devices, Chem. Rev. **120**, 7399 (2020).

[18] B. T. Spann, J. C. Weber, M. D. Brubaker, T. E. Harvey, L. Yang, H. Honarvar, C. N. Tsai, A. C. Treglia, M. Lee, M. I. Hussein, and K. A. Bertness, Semiconductor thermal and electrical properties decoupled by localized phonon resonances, Adv. Mater. Interfaces **35**, 2209779 (2023).

[19] X. W. Zhou, R. E. Jones, C. J. Kimmer, J. C. Duda, and P. E. Hopkins, Relationship of thermal boundary conductance to structure from an analytical model plus molecular dynamics simulations, Phys. Rev. B **87**, 094303 (2013).

[20] X. Wei, T. Zhang, and T. Luo, Thermal energy transport across hard–soft interfaces, ACS Energy Lett. **2**, 2283 (2017).

[21] X. Ran, Y. Guo, and M. Wang, Interfacial phonon transport with frequency-dependent transmissivity by Monte Carlo simulation, Int. J. Heat Mass Transfer **123**, 616 (2018).

[22] Y.-C. Hua and B.-Y. Cao, Study of phononic thermal transport across nanostructured interfaces using phonon Monte Carlo method, Int. J. Heat Mass Transfer **154**, 119762 (2020).

[23] S. Jin, Z. Zhang, Y. Guo, J. Chen, M. Nomura, and S. Volz, Optimization of interfacial thermal transport in Si/Ge heterostructure driven by machine learning, Int. J. Heat Mass Transfer **182**, 122014 (2022).

[24] H. Han, Y. Zhang, N. Wang, M. K. Samani, Y. Ni, Z. Y. Mijbil, M. Edwards, S. Xiong, K. Saaskilahti, M. Murugesan, Y. Fu, L. Ye, H. Sadeghi, S. Bailey, Y. A. Kosevich, C. J. Lambert, J. Liu, and S. Volz, Functionalization mediates heat transport in graphene nanoflakes, Nat. Commun. **7**, 11281 (2016).

[25] T. Luo and J. R. Lloyd, Enhancement of thermal energy transport across graphene/graphite and polymer interfaces: A molecular dynamics study, Adv. Funct. Mater. **22**, 2495 (2012).

[26] M. Hu and D. Poulikakos, Graphene mediated thermal resistance reduction at strongly coupled interfaces, Int. J. Heat Mass Transfer **62**, 205 (2013).

[27] Y. Ma, Z. Zhang, J. Chen, K. Sääskilahti, S. Volz, and J. Chen, Ordered water layers by interfacial charge decoration leading to an ultra-low Kapitza resistance between graphene and water, Carbon **135**, 263 (2018).

[28] B. Gotsmann and M. A. Lantz, Quantized thermal transport across contacts of rough surfaces, Nat. Mater. **12**, 59 (2013).

[29] J. Chen, J. H. Walther, and P. Koumoutsakos, Strain engineering of Kapitza resistance in few-layer graphene, Nano Lett. **14**, 819 (2014).

[30] D. Alexeev, J. Chen, J. H. Walther, K. P. Giapis, P. Angelikopoulos, and P. Koumoutsakos, Kapitza resistance between few-layer graphene and water: Liquid layering effects, Nano Lett. **15**, 5744 (2015).

[31] X. D. Zhang, G. Yang, and B. Y. Cao, Bonding-enhanced interfacial thermal transport: Mechanisms, materials, and applications, Adv. Mater. Interfaces **9**, 2200078 (2022).

[32] K. Gordiz and A. Henry, Phonon transport at interfaces: Determining the correct modes of vibration, J. Appl. Phys. **119**, 015101 (2016).

[33] K. Gordiz and A. Henry, Phonon transport at crystalline Si/Ge interfaces: The role of interfacial modes of vibration, Sci. Rep. **6**, 23139 (2016).

[34] K. Gordiz and A. Henry, Phonon transport at interfaces between different phases of silicon and germanium, J. Appl. Phys. **121**, 025102 (2017).

[35] T. Feng, Y. Zhong, J. Shi, and X. Ruan, Unexpected high inelastic phonon transport across solid-solid interface: Modal nonequilibrium molecular dynamics simulations and Landauer analysis, Phys. Rev. B **99**, 045301 (2019).

[36] K. Gordiz, M. G. Muraleedharan, and A. Henry, Interface conductance modal analysis of a crystalline Si-amorphous SiO_2 interface, J. Appl. Phys. **125**, 135102 (2019).

[37] Z. Cheng, R. Li, X. Yan, G. Jernigan, J. Shi, M. E. Liao, N. J. Hines, C. A. Gadre, J. C. Idrobo, E. Lee, K. D. Hobart, M. S. Goorsky, X. Pan, T. Luo, and S. Graham, Experimental observation of localized interfacial phonon modes, Nat. Commun. **12**, 6901 (2021).

[38] R. Qi, R. Shi, Y. Li, Y. Sun, M. Wu, N. Li, J. Du, K. Liu, C. Chen, J. Chen, F. Wang, D. Yu, E. G. Wang, and P. Gao, Measuring phonon dispersion at an interface, Nature (London) **599**, 399 (2021).

[39] H. Zhou, G. Zhang, and Y.-W. Zhang, Effects of localized phonons on interfacial thermal conductance, Phys. Rev. B **106**, 195435 (2022).

[40] A. Giri, S. W. King, W. A. Lanford, A. B. Mei, D. Merrill, L. Y. Li, R. Oviedo, J. Richards, D. H. Olson, J. L. Braun, J. T. Gaskins, F. Deangelis, A. Henry, and P. E. Hopkins, Interfacial defect vibrations enhance thermal transport in amorphous multilayers with ultrahigh thermal boundary conductance, Adv. Mater. **30**, e1804097 (2018).

[41] S. Plimpton, Fast parallel algorithms for short-range molecular dynamics, J. Comput. Phys. **117**, 1 (1995).

[42] Z. Fan, T. Siro, and A. Harju, Accelerated molecular dynamics force evaluation on graphics processing units for thermal conductivity calculations, Comput. Phys. Commun. **184**, 1414 (2013).

[43] Z. Fan, Y. Wang, P. Ying, K. Song, J. Wang, Y. Wang, Z. Zeng, K. Xu, E. Lindgren, J. M. Rahm, A. J. Gabourie, J. Liu, H. Dong, J. Wu, Y. Chen, Z. Zhong, J. Sun, P. Erhart, Y. Su, and T. Ala-Nissila, GPUMD: A package for constructing accurate machine-learned potentials and performing highly efficient atomistic simulations, J. Chem. Phys. **157**, 114801 (2022).

[44] F. H. Stillinger and T. A. Weber, Computer simulation of local order in condensed phases of silicon, Phys. Rev. B **31**, 5262 (1985).

[45] T. Murakami, T. Hori, T. Shiga, and J. Shiomi, Probing and tuning inelastic phonon conductance across finite-thickness interface, Appl. Phys. Express **7**, 121801 (2014).

[46] C. H. Baker and P. M. Norris, Effect of long- and short-range order on SiGe alloy thermal conductivity: Molecular dynamics simulation, Phys. Rev. B **91**, 180302 (2015).

[47] S. Hu, H. Zhang, S. Xiong, H. Zhang, H. Wang, Y. Chen, S. Volz, and Y. Ni, Screw dislocation induced phonon transport suppression in SiGe superlattices, Phys. Rev. B **100**, 075432 (2019).

[48] S. Hu, L. Feng, C. Shao, I. A. Strelnikov, Y. A. Kosevich, and J. Shiomi, Two-path phonon interference resonance induces a stop band in a silicon crystal matrix with a multilayer array of embedded nanoparticles, Phys. Rev. B **102**, 024301 (2020).

[49] See Supplemental Material at http://link.aps.org/supplemental/10.1103/PhysRevB.108.235426 for comprehensive details on additional MD simulations, the NEP potential training process, the heat flux and temperature profile, size effects, resonance hybridization, elastic and inelastic contributions, as well as the interfacial modes. The Supplemental Material also contains Refs. [84–90].

[50] K. Sääskilahti, J. Oksanen, S. Volz, and J. Tulkki, Frequency-dependent phonon mean free path in carbon nanotubes from nonequilibrium molecular dynamics, Phys. Rev. B **91**, 115426 (2015).

[51] K. Sääskilahti, J. Oksanen, J. Tulkki, and S. Volz, Spectral mapping of heat transfer mechanisms at liquid-solid interfaces, Phys. Rev. E **93**, 052141 (2016).

[52] Y. Imry and R. Landauer, Conductance viewed as transmission, Rev. Mod. Phys. **71**, S306 (1999).

[53] D. A. Young and H. J. Maris, Lattice-dynamical calculation of the Kapitza resistance between fcc lattices, Phys. Rev. B **40**, 3685 (1989).

[54] Z. Li, S. Xiong, C. Sievers, Y. Hu, Z. Fan, N. Wei, H. Bao, S. Chen, D. Donadio, and T. Ala-Nissila, Influence of thermostatting on nonequilibrium molecular dynamics simulations of heat conduction in solids, J. Chem. Phys. **151**, 234105 (2019).

[55] J. Chen, G. Zhang, and B. Li, Tunable thermal conductivity of $Si_{1-x}Ge_x$ nanowires, Appl. Phys. Lett. **95**, 073117 (2009).

[56] J. Shi, Y. Dong, T. Fisher, and X. Ruan, Thermal transport across carbon nanotube-graphene covalent and van der Waals junctions, J. Appl. Phys. **118**, 044302 (2015).

[57] S.-W. Hung, S. Hu, and J. Shiomi, Spectral control of thermal boundary conductance between copper and carbon arbon crystals by self-assembled monolayers, ACS Appl. Electron. Mater. **1**, 2594 (2019).

[58] X. Liu, G. Zhang, and Y. W. Zhang, Topological defects at the graphene/h-BN interface abnormally enhance its thermal conductance, Nano Lett. **16**, 4954 (2016).

[59] X. Liu, J. Gao, G. Zhang, and Y.-W. Zhang, MoS_2-graphene in-plane contact for high interfacial thermal conduction, Nano Res. **10**, 2944 (2017).

[60] Q. Wang, J. Zhang, Y. Xiong, S. Li, V. Chernysh, and X. Liu, Atomic-scale surface engineering for giant thermal transport enhancement across 2D/3D van der Waals interfaces, ACS Appl. Mater. Interfaces **15**, 3377 (2023).

[61] B. Li, J. Lan, and L. Wang, Interface thermal resistance between dissimilar anharmonic lattices, Phys. Rev. Lett. **95**, 104302 (2005).

[62] Z. Liang, K. Sasikumar, and P. Keblinski, Thermal transport across a substrate-thin-film interface: Effects of film thickness and surface roughness, Phys. Rev. Lett. **113**, 065901 (2014).

[63] X. K. Chen, M. Pang, T. Chen, D. Du, and K. Q. Chen, Thermal rectification in asymmetric graphene/hexagonal boron nitride van der Waals heterostructures, ACS Appl. Mater. Interfaces **12**, 15517 (2020).

[64] J. D. Gale, GULP: A computer program for the symmetry-adapted simulation of solids, J. Chem. Soc., Faraday Trans. **93**, 629 (1997).

[65] D. Ma, Y. Zhao, and L. Zhang, Facilitating thermal transport across Si/Ge interface via mass-graded interlayer: The role of elastic and inelastic phonon processes, J. Appl. Phys. **129**, 175302 (2021).

[66] Z. Fan, Z. Zeng, C. Zhang, Y. Wang, K. Song, H. Dong, Y. Chen, and T. Ala-Nissila, Neuroevolution machine learning potentials: Combining high accuracy and low cost in atomistic simulations and application to heat transport, Phys. Rev. B **104**, 104309 (2021).

[67] K. Xu, A. J. Gabourie, A. Hashemi, Z. Fan, N. Wei, A. B. Farimani, H.-P. Komsa, A. V. Krasheninnikov, E. Pop, and T. Ala-Nissila, Thermal transport in MoS_2 from molecular dynamics using different empirical potentials, Phys. Rev. B **99**, 054303 (2019).

[68] R. J. Stoner and H. J. Maris, Kapitza conductance and heat flow between solids at temperatures from 50 to 300 K, Phys. Rev. B **48**, 16373 (1993).

[69] H.-K. Lyeo and D. G. Cahill, Thermal conductance of interfaces between highly dissimilar materials, Phys. Rev. B **73**, 144301 (2006).

[70] Q. Li, F. Liu, S. Hu, H. Song, S. Yang, H. Jiang, T. Wang, Y. K. Koh, C. Zhao, F. Kang, J. Wu, X. Gu, B. Sun, and X. Wang, Inelastic phonon transport across atomically sharp metal/semiconductor interfaces, Nat. Commun. **13**, 4901 (2022).

[71] C. A. Bryant and P. H. Keesom, Low-temperature specific heat of germanium, Phys. Rev. **124**, 698 (1961).

[72] J. Dunn, E. Antillon, J. Maassen, M. Lundstrom, and A. Strachan, Role of energy distribution in contacts on thermal transport in Si: A molecular dynamics study, J. Appl. Phys. **120**, 225112 (2016).

[73] T. Feng, W. Yao, Z. Wang, J. Shi, C. Li, B. Cao, and X. Ruan, Spectral analysis of nonequilibrium molecular dynamics: Spectral phonon temperature and local nonequilibrium in thin films and across interfaces, Phys. Rev. B **95**, 195202 (2017).

[74] X. Li, J. Han, and S. Lee, Thermal resistance from non-equilibrium phonons at Si–Ge interface, Mater. Today Phys. **34**, 101063 (2023).

[75] S. Hu, C. Zhao, and X. Gu, Phonon non-equilibrium effects on interface thermal resistance between graphene and substrates, Int. J. Therm. Sci. **196**, 108725 (2024).

[76] W. Zheng, C. J. McClellan, E. Pop, and Y. K. Koh, Nonequilibrium phonon thermal resistance at MoS_2/oxide and graphene/oxide interfaces, ACS Appl. Mater. Interfaces **14**, 22372 (2022).

[77] B. Xu, S. Hu, S. W. Hung, C. Shao, H. Chandra, F. R. Chen, T. Kodama, and J. Shiomi, Weaker bonding can give larger thermal conductance at highly mismatched interfaces, Sci. Adv. **7**, eabf8197 (2021).

[78] Y. Wang and P. Keblinski, Role of wetting and nanoscale roughness on thermal conductance at liquid-solid interface, Appl. Phys. Lett. **99**, 073112 (2011).

[79] S. Merabia and K. Termentzidis, Thermal boundary conductance across rough interfaces probed by molecular dynamics, Phys. Rev. B **89**, 054309 (2014).

[80] L. Qiu, F. Li, N. Zhu, Y. Feng, X. Zhang, and X. Zhang, Elaborate manipulation on CNT intertube heat transport by using a polymer knob, Int. J. Heat Mass Transfer **184**, 122280 (2022).

[81] Z. Ding, Q.-X. Pei, J.-W. Jiang, W. Huang, and Y.-W. Zhang, Interfacial thermal conductance in graphene/MoS_2 heterostructures, Carbon **96**, 888 (2016).

[82] E. Lee, T. Zhang, T. Yoo, Z. Guo, and T. Luo, Nanostructures significantly enhance thermal transport across solid interfaces, ACS Appl. Mater. Interfaces **8**, 35505 (2016).

[83] L. Yang, X. Wan, D. Ma, Y. Jiang, and N. Yang, Maximization and minimization of interfacial thermal conductance by modulating the mass distribution of the interlayer, Phys. Rev. B **103**, 155305 (2021).

[84] K. Xu, S. Deng, T. Liang, X. Cao, M. Han, X. Zeng, Z. Zhang, N. Yang, and J. Wu, Efficient mechanical modulation of the phonon thermal conductivity of Mo_6S_6 nanowires, Nanoscale **14**, 3078 (2022).

[85] Y. Yao, G. Ren, Y. Yu, J. Che, T. Liang, L. Li, Y. Liu, F. Yang, and X. Zhao, Thermal conduction mechanism of ferroelastic Zr-Y-Yb-Ta-Nb-O high-entropy oxides with glass-like thermal conductivity, J. Am. Ceram. Soc. **105**, 4360 (2022).

[86] P. Ying, H. Dong, T. Liang, Z. Fan, Z. Zhong, and J. Zhang, Atomistic insights into the mechanical anisotropy and fragility of monolayer fullerene networks using quantum mechanical calculations and machine-learning molecular dynamics simulations, Extreme Mech. Lett. **58**, 101929 (2023).

[87] G. Nilsson and G. Nelin, Study of the homology between silicon and germanium by thermal-neutron spectrometry, Phys. Rev. B **6**, 3777 (1972).

[88] A. Ward and D. A. Broido, Intrinsic phonon relaxation times from first-principles studies of the thermal conductivities of Si and Ge, Phys. Rev. B **81**, 085205 (2010).

[89] G. Nilsson and G. Nelin, Phonon dispersion relations in Ge at 80 °K, Phys. Rev. B **3**, 364 (1971).

[90] A. Trejo, J. L. Cuevas, R. Vázquez-Medina, and M. Cruz-Irisson, Phonon band structure of porous Ge from *ab initio* supercell calculation, Microelectron. Eng. **90**, 141 (2012).